Iran J Radiol. 2016 April; 13(2):e23026. doi: 10.5812/iranjradiol.23026.

Published online 2016 February 27. **Research Article**

Diagnostic Accuracy of Dynamic Contrast Enhanced Magnetic Resonance Imaging in Characterizing Lung Masses

Nagihan Inan,[1,*] Arzu Arslan,[1] Muhammed Donmez,[1] and Hasan Tahsin Sarisoy[1]

[1]Department of Radiology, School of Medicine, University of Kocaeli, Kocaeli, Turkey

[*]*Corresponding author*: Nagihan Inan, Department of Radiology, School of Medicine, University of Kocaeli, Kocaeli, Turkey. Tel: +90-2623037242, Fax: +90-2623038003, E-mail: nagihaninan@yahoo.com.tr

Received 2014 August 24; **Revised** 2014 October 02; **Accepted** 2014 December 14.

Abstract

Background: Imaging plays a critical role not only in the detection, but also in the characterization of lung masses as benign or malignant.
Objectives: To determine the diagnostic accuracy of dynamic magnetic resonance imaging (MRI) in the differential diagnosis of benign and malignant lung masses.
Patients and Methods: Ninety-four masses were included in this prospective study. Five dynamic series of T1-weighted spoiled gradient echo (FFE) images were obtained, followed by a T1-weighted FFE sequence in the late phase (5_{th} minutes). Contrast enhancement patterns in the early (25_{th} second) and late (5_{th} minute) phase images were evaluated. For the quantitative evaluation, signal intensity (SI)-time curves were obtained and the maximum relative enhancement, wash-in rate, and time-to-peak enhancement of masses in both groups were calculated.
Results: The early phase contrast enhancement patterns were homogeneous in 78.2% of the benign masses, while heterogeneous in 74.4% of the malignant tumors. On the late phase images, 70.8% of the benign masses showed homogeneous enhancement, while most of the malignant masses showed heterogeneous enhancement (82.4%). During the first pass, the maximum relative enhancement and wash-in rate values of malignant masses were significantly higher than those of the benign masses (P = 0.03 and 0.04, respectively). The cutoff value at 15% yielded a sensitivity of 85.4%, specificity of 61.2%, and positive predictive value of 68.7% for the maximum relative enhancement.
Conclusion: Contrast enhancement patterns and SI-time curve analysis of MRI are helpful in the differential diagnosis of benign and malignant lung masses.

Keywords: Lung, Neoplasm, Contrast Enhancement, Dynamic Imaging, Magnetic Resonance Imaging

1. Background

Imaging plays a critical role not only in the detection, but also in the characterization of lung masses as benign or malignant. As the therapy depends on the nature of the mass, a lung mass detected in a patient requires careful differential diagnosis to choose the optimal treatment for each patient. The growth rate of the mass on low-dose computed tomography (CT) and the metabolic uptake of fluorodeoxyglucose (FDG) on positron emission tomography (PET)-CT are two different non-invasive current acceptable imaging modalities (1, 2). However, these two methods have increased radiation exposure. In addition, the sensitivity of PET-CT is low in nodules smaller than 20 mm (2, 3). Therefore, another non-invasive method is required in the differential diagnosis of indistinct lung masses to avoid unnecessary biopsies that carry potential risks. Over the years, the imaging rates have increased with the development of new techniques such as multidetector CT (MDCT) and gradient echo (GRE) magnetic resonance imaging (MRI) techniques (4, 5). In the recent years, a few recent reports suggested that dynamic contrast-enhanced imaging with MDCT or MRI might be helpful in this regard (6-8). Incremental acquisitions with an interval of 1 minute were used in studies with CT (6, 9, 10). However, a higher temporal resolution is necessary to evaluate the first pass of the contrast agent. This is possible with CT, but there is very high radiation exposure (9, 10). As a result, MRI seems to have the potential utility for evaluating the first pass.

2. Objectives

The purpose of this study was to evaluate the diagnostic accuracy of contrast wash-in patterns on dynamic (0 - 100 seconds) spoiled GRE MRI for the differentiation of lung masses, by both quantitative and qualitative analysis.

3. Patients and Methods

3.1. Patients Selection

The study protocol was approved by our institutional review board for human investigations, and informed consent was obtained from all patients. The sample sizes were determined for a study (4) with 95% power. Between April 2012 and May 2013, 94 lung masses in 66 consecutive patients (23 females, 43 males) detected by CT of the thorax were included in this prospective study. Patients were selected according to the following criteria: a, presence of a newly detected mass; b, absence of calcification or definite fat attenuation of the mass at CT; c, absence of contraindication to administration of contrast material. Because of the limited resolution of the MR imaging, eight lesions (six patients) smaller than 1 cm in diameter were not included. Seven metastases (seven patients) were excluded because of insufficient histopathological diagnosis. Four claustrophobic patients also had to be excluded from the study. Thus, 49 patients (14 females, 35 males) with 75 lung masses were enrolled into the study and were examined by dynamic MRI at our hospital.

Diagnosis of the primary malignant masses was confirmed by either biopsy or surgery. All of the solitary pulmonary nodules, fibrosis, and atelectasis with a tentative radiological diagnosis of benign mass showed no change in either clinical or radiological (CT every 6 months) follow-ups (6 - 15 months). A patient with infarcts and a patient with acute pneumonic consolidation had typical clinical, laboratory, and radiologic findings. Diagnosis of the hydatic cysts (HCs) was confirmed by positive serology for hydatidosis (hemaglutinin inhibition).

3.2. MR Imaging

All patients were examined with a 1.5 Tesla MR scanner (Gyroscan Intera; Philips medical systems, Eindhoven, The Netherlands) using a four-element phased-array body coil. This system had a maximal gradient strength of 30 mT/m and a slew rate of 150 mT/m/ms. All patients were examined initially with the routine MR imaging protocol for the thorax that included precontrast axial T1-weighted (W) breath-hold spoiled gradient echo (fast field echo: FFE) with and without fat suppression (TR/TE/FA/NEX:169/4.6/80/1), coronal and axial T2-W single shot turbo spin echo (SS-TSE) (TR/TE/NEX/TSE factor: 700/80/1/72), and axial T2-W SS-TSE with fat suppression (TR/TE/NEX/TSE factor: 700/80/1/72). Subsequently, 0.1 mmol/kg Gd-DTPA (Magnevist, Schering, Germany) was administered as a hand-injected bolus in 5 seconds followed by a rapid flush with 10 - 20 mL of saline. Five dynamic series of T1-W breath-hold FFE (TR/TE/FA:169/4.6/80) images were acquired at 0_{th}, 25_{th}, 50_{th}, 75_{th} and 100_{th} seconds and an additional late phase (5_{th} minute) imaging was performed with fat suppressed axial T1-weighted breath-hold FFE sequence (TR/TE/FA/NEX:169/4.6/80/1). The scan was initiated simultaneously with the start of contrast injection. Imaging included a multi-section acquisition with a slice thickness of 4 mm, an intersection gap of 0.4 mm, and an acquisition matrix of 256×512. The field of view varied between 455 and 500 mm. All sequences were acquired using a partially parallel imaging acquisition and sensitivity encoding (SENSE) reconstruction with a reduction factor (R) of 2. Total imaging time was 15 - 20 minutes.

3.3. Image Analysis

The visual evaluation was determined by two radiologists (N.I., H.T.S.) with 10 and 12 years of experience in chest radiology. The radiologists were blinded to the clinical history, results of the prior imaging studies, and the pathology. The raters were also blinded to the other rater's scores. All the quantitative measurements were done by one of the radiologists (N.I.) on the computer workstation using a region of interest (ROI). The ROI was placed manually in the center of the tumor, with an effort to avoid interference from the surrounding lung tissue and vascular structure. The size of the ROI was kept as large as possible, covering at least two thirds of the masses. The average of the two consecutive measurements was recorded as the final value.

3.3.1. Visual Evaluation

On precontrast conventional T1-and T2-W images; the contours, internal structure, and signal intensities (SIs) of the masses were visually assessed. On post contrast images, contrast enhancement patterns in the early (25_{th} second) and late phase (5_{th} minute) images were evaluated visually. The contrast enhancement patterns in the early phase were classified into two categories: 1, homogeneous; 2, heterogeneous. Homogeneous enhancement refers to a uniform increase in the signal intensity. Heterogeneous enhancement refers to an enhancement in which the irregular portion of the mass demonstrates lesser signal intensity. The late phase images were examined for presence of contrast enhancement in the periphery and or in the center of the masses and the lesions were classified into three categories: 1, peripheral; 2, homogeneous; 3, heterogeneous. Peripheral enhancement (PE) refers to lesions with a central contrast washout. Heterogeneous enhancement refers to residual contrast either in the periphery or center of the masses. Homogeneous enhancement refers to homogeneous signal in the late phase.

3.3.2. Quantitative Evaluation

Quantitative evaluation was performed by obtaining SI-time curves and calculating the wash-in rate (WIR), max-

imum relative enhancement (MRE), and time-to-peak (TTP) enhancement of the masses, automatically on the workstation (Dell workstation precision 650, view forum release 3.4 system) according to the following formulas.

$$\mathrm{MRE} = \frac{\mathrm{SI\ lesion}_{\mathrm{maximum}} - \mathrm{SI\ lesion}_{t0}}{\mathrm{SI\ lesion}_{t0}} \times 100 \quad (1)$$

The relative MR SI is measured at five time points along the enhancement curve (postcontrast 0_{th}, 25_{th}, 50_{th}, 75_{th}, 100_{th} seconds).

WIR is defined as the maximum SI gradient that can be calculated between successive time points with the following formula.

$$\mathrm{Wash-in\ Rate} = \mathrm{MAX}\left(\frac{S_i - S_{i-1}}{t_i - t_{i-1}}\right) \quad (2)$$

(S_i and S_{i-1} are the measured SIs at consecutive time points t_i and t_{i-1}, respectively).

3.4. Statistical Analysis

Inter- and intra-observer agreements in the interpretation were evaluated and reported using Kappa (K) coefficient statistics and its 95% confidence interval (CI). The guidelines of Landis and Koch were followed in interpreting Kappa values: 0.00 - 0.20, slight agreement; 0.21 - 0.40, fair agreement; 0.41 - 0.60, moderate agreement; 0.61 - 0.80, substantial agreement; and 0.81 - 1.00, almost perfect agreement.

The fitness of numeric data set to normal distribution was determined by Kolmogorov-Smirnov test. The statistical significance of the differences in WIRs, MREs, and TTPs were analyzed by student t test. A $P < 0.05$ was considered as statistical significance. To evaluate the diagnostic performance of the quantitative tests for differentiating benign and malignant masses and to describe the sensitivity and specificity of the tests, receiver-operating characteristic (ROC) analysis was performed. The areas and standard errors for each ROC curve were calculated by the method described by Metz (11). The area under the ROC curve reflects the performance of the tests. The optimum cut-off point was determined as the best discriminative value between the two groups in terms of maximum sensitivity and minimum false-positive result. All statistical analyses were performed using SPSS ver. 20 (IBM Corp. Released 2011. IBM SPSS statistics for windows, Armonk, NY, USA) software.

4. Results

During the study period, a total of 49 patients (14 females, 35 males) with 75 lung masses met our inclusion criteria and all patients were examined by dynamic MRI. Of the masses, 35 (in 24 patients; 4 females, 20 males) were malignant and 40 (in 25 patients; 10 females, 15 males) were benign. The malignant masses consisted of 30 primary malignant tumors (eight adenocarcinomas, six squamous-cell carcinomas, 12 non-small cell carcinomas, three small cell carcinomas, and one schwannoma) and five lymphadenopathies. The benign masses consisted of 12 benign solitary pulmonary nodules, 19 post-obstructive atelectasis, three parenchymal fibrosis, three infarcts, two HCs, and one acute pneumonic consolidation.

The mean diameter for malignant and benign masses was 32.12 $\pm$ 21.75 mm and 52.63 $\pm$ 21.78 mm, respectively. The mean age of the patients was 54 $\pm$ 13 years. Most of the malignant masses were located in the right lung (76%), especially the middle lobe (31%) or superior segment of the lower lobe (12%). Benign masses showed an approximate equal distribution (49.4% were located in the right lung and 50.6% were located in the left lung).

4.1. Visual Evaluation

Results of the visual evaluation of the SIs and morphologic features of the masses are shown in Table 1. The pre contrast morphologic features and SIs showed substantial to almost perfect inter-observer agreement. The highest agreement was found in contour (K = 0.85) (95% CI: 0.80 - 0.92). Furthermore, the agreement for SIs and internal structure were found as substantial (K = 0.66, K = 0.68) (95% CI: 0.60 - 0.72; 0.61 - 0.76). Most of the benign masses had smooth margins and homogeneous internal structures (Figure 1). On the other hand, most of the malignant masses had irregular margins (Figure 2). There were no significant differences of SIs on T1 and T2W images.

Visual evaluation of the contrast enhancement patterns of the benign and malignant masses in the early (25_{th} second) and late (5_{th} minute) phases are shown in Table 2. The inter-observer agreement for the early (homogeneous and heterogeneous) and late phase (homogeneous, heterogeneous, and peripheral enhancement) contrast enhancement patterns was found as almost perfect (K = 0.91, K = 0.94, K = 0.83, K = 0.94, K = 0.94) (95% CI: 0.88 - 0.95; 0.90 - 0.98; 0.75 - 0.92; 0.90 - 0.98; 0.90 - 0.99). In the early phase, most of the benign masses (78.2%) showed homogeneous enhancement, while most of the malignant masses showed heterogeneous (74.4%) enhancement. In the late phase, while 70.8% of the benign masses had homogeneous enhancement and 18.8% had PE, most of the malignant masses (82.4%) had central heterogeneous enhancement.

4.2. Quantitative Evaluation

Results of the quantitative analysis of the dynamic contrast enhanced MR images are reviewed in Table 3. The

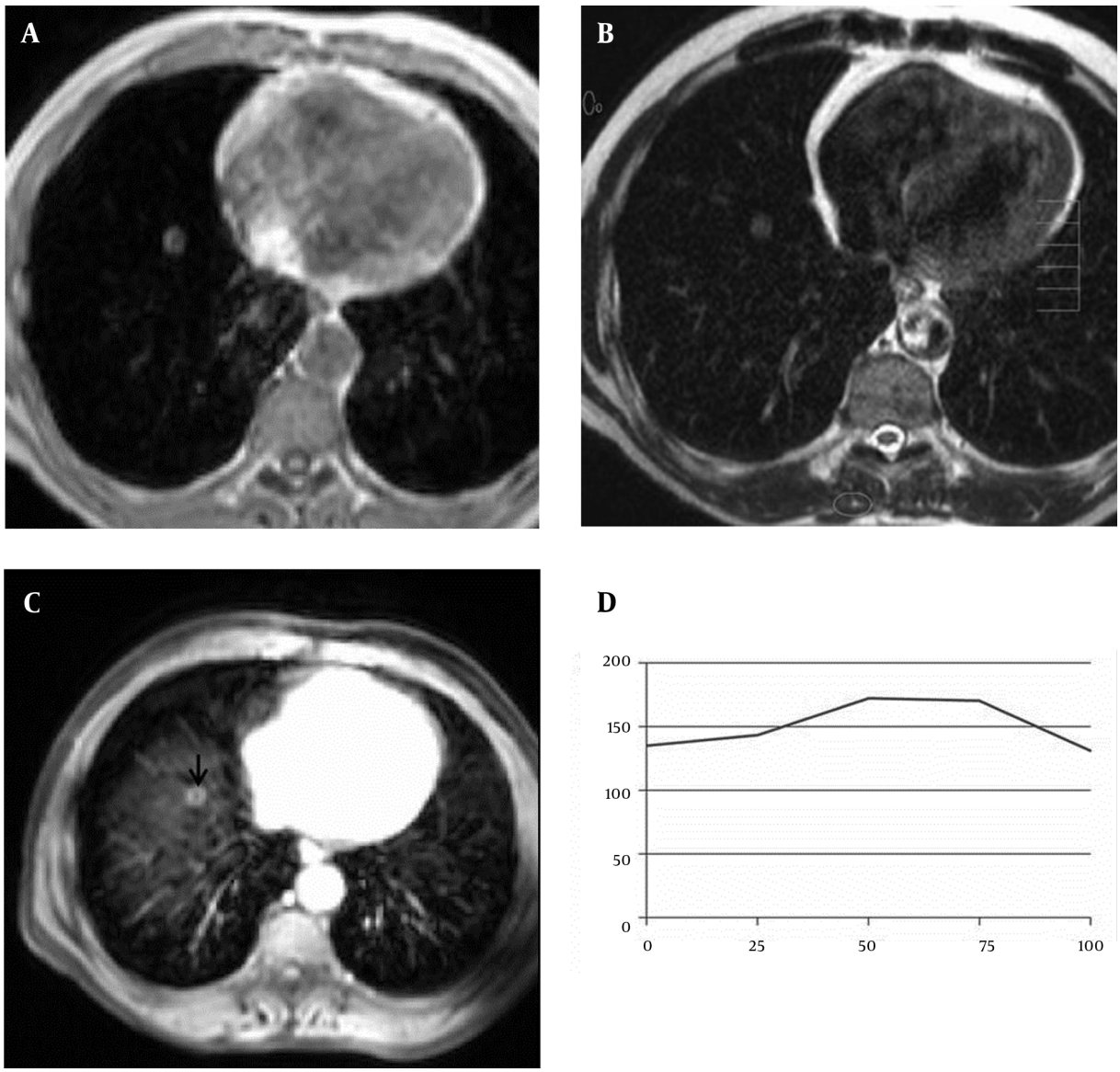

Figure 1. A 61-year-old man with benign solitary pulmonary nodule. A, Axial T1-weighted FFE and B, T2-weighted TSE MR images show a nodule in the right lower lobe of the lung. C, This nodule (arrow) shows peripheral ring-enhancement on the axial post contrast fat-suppressed T1-weighted image (5_{th} minute). D, SI-time curve and quantitative interpretation of the curve obtained from the nodule. Maximun relative enhancement (27%) and wash-in rate (1.48 seconds) implied benign mass.

intra-observer agreement for measurements of WIR, MRE, and TTP were found as almost perfect (K= 0.86, K= 0.94, K= 0.94) (95% CI: 0.81 - 0.91; 0.88 - 0.98; 0.89 - 0.98) which indicates satisfactory reliability. WIR of the malignant masses were significantly higher than that of the benign masses (P = 0.046) (Table 3). The area under the ROC curve was 0.619 ± 0.062 (95% CI: 0.58 - 0.65). However, we could not obtain a sufficiently discriminative cut-off value by ROC analysis. MRE of the malignant masses were significantly higher than the benign masses (P = 0.038). The best discriminative parameter was MRE. The area under the ROC was 0.683 ± 0.059 (95% CI: 0.65 - 0.72). Setting the cut-off value at 15%, we found a sensitivity of 85.4% (95% CI: 0.81 - 0.89), a specificity of 61.2% (95% CI: 0.50 - 0.71), and a positive predictive value (PPV) of 68.7% (95% CI: 0.62 - 0.74) for the MRE. The malignant masses showed a longer but statistically insignificant TTP compared to the benign masses. When we analyzed subgroups of the masses, except for HCs, there were no significant differences among the groups.

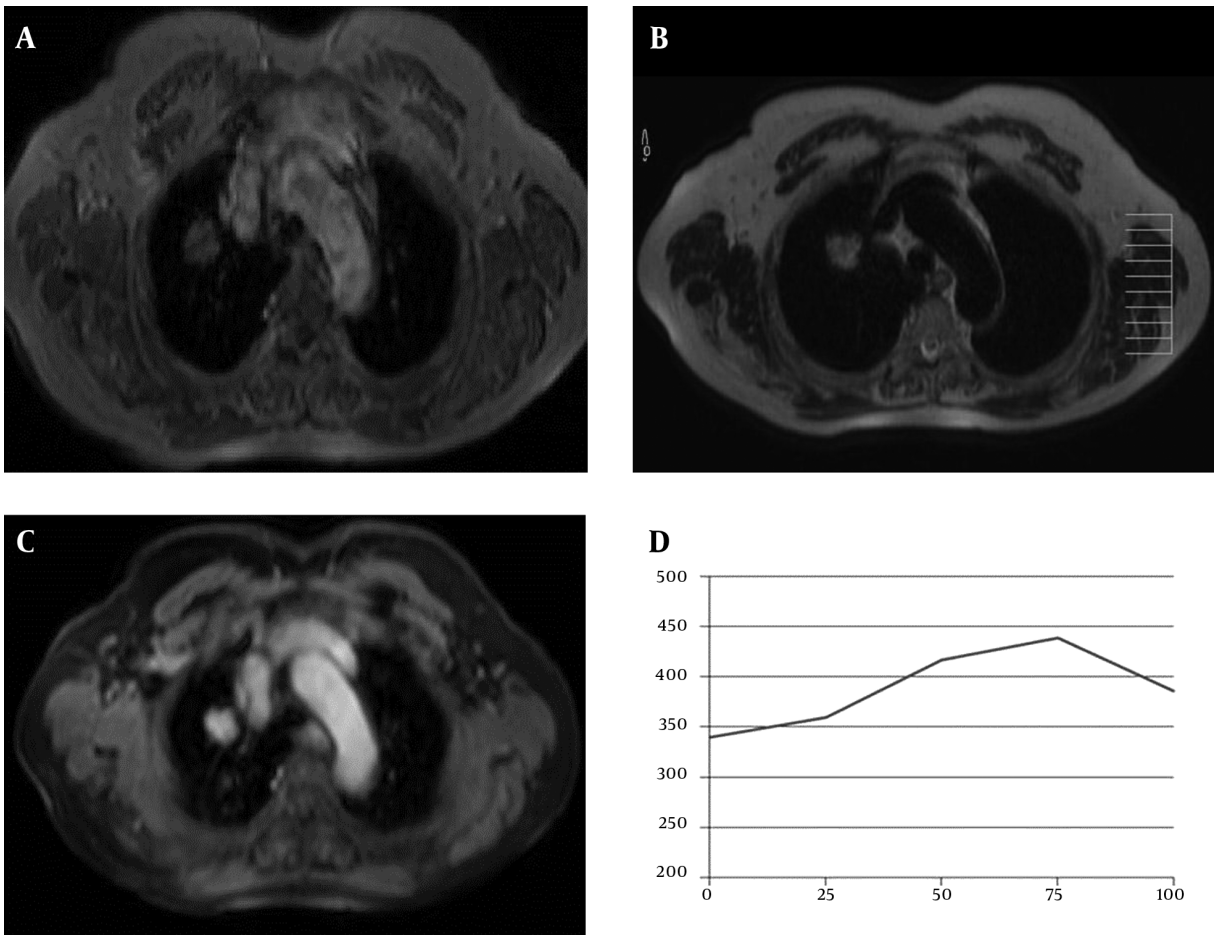

Figure 2. A 77-year-old woman with adenocarcinoma. A, Axial T1-weighted FFE and B, T2-weighted TSE, MR images show a mass in the right upper lobe of the lung; C, This mass shows prominent central homogeneous enhancement on the axial post contrast fat-suppressed T1-weighted image (5_{th} minute); D, SI-time curve and quantitative interpretation of the curve obtained from the mass. Maximum relative enhancement (30%) and wash-in rate (2.28 seconds) implied benign mass.

5. Discussion

Dynamic contrast enhanced imaging on MRI using spoiled GRE sequence have been widely used for characterization of many lesions as benign and malignant such us adrenal (12), pancreas (13), liver (14), and breast masses (15). The main advantages of this sequence is its ability to acquire a data set rapidly during a single breath-hold to allow dynamic imaging with reduced motion artifacts resulting in an increased quality of images.

The contrast enhancement patterns and kinetic parameters vary on CT and MRI studies; hence, results of these two methods are not comparable. Because while the contrast enhancement on CT examination is affected by concentration of contrast, the enhancement on MRI is affected by the vascularity, capillary permeability, and volume of the extracellular space (4, 16). These features reflect the nature of the masses. On MRI, during the first pass, approximately 50% of the contrast agent enters the interstitial space through the capillary network (17). Rapid and strong enhancement is related to rich vascularity and increased permeability of capillaries resulting in interstitial accumulation of the contrast (18, 19). On the basis of these findings, malignant lung masses must show strong enhancement with faster wash-in (20-24). In our study, malignant masses showed higher MRE and WIR than benign masses as expected. The sensitivity, specificity, and PPV of dynamic images were 85.4%, 61.2%, and 68.7%, respectively by using a threshold value of 15% for MRE. Our results are slightly lower than some previous studies with CT (5) and MRI (19). For example, in a previous report using dynamic MRI, the sensitivity, specificity, and accuracy were reported as 100%, 70%, and 95%, respectively for a threshold value of 15% for MRE (19). In another previous report

Table 1. Visual Evaluation of Signal Intensities and Morphologic Features of the Masses on Precontrast Conventional T1 and T2W Images[a]

	Benign Masses	Malignant Masses
Number	40	35
Size (mm), mean (SD)	32.12 (21.75)	52.63 (21.78)
Contour		
Smooth	81.2	22.8
Irregular	18.8	77.2
Internal structure		
Homogeneous	89.7	45.7
Heterogeneous	10.3	54.3
Signal Intensity on T1W image		
Hypointense	22.7	20.3
Isointense	52.5	75.2
Hyperintense	24.8	4.5
Signal Intensity on T2W image		
Hypointense	-	-
Isointense	17.2	3.2
Hyperintense	82.8	96.8

[a]Values are expressed as % unless otherwise indicated.

Table 2. Visual Evaluation of Contrast Enhancement Patterns of the Masses on Post contrast MR Images at 25th Second and 5th Minute[a]

	Benign Masses	Malignant Masses
Number	40	35
25th second		
Homogeneous	78.2	25.6
Heterogeneous	21.8	74.4
5th minute		
Homogeneous	70.8	10.6
Heterogeneous	10.4	82.4
PE	18.8	7.0

Abbreviation: PE, peripheral enhancement.
[a]Values are expressed as %.

Table 3. Quantitative Analysis of Dynamic Contrast Enhanced Magnetic Resonance Imaging of Lung Masses

	Malignant Masses	Benign Masses	P Value
WIR	2.25 (5.15)	2.45 (2.28)	0.046
MRE	26.34 (24.81)	43.21 (32.52)	0.038
TTP	63.65 (33.72)	73.36 (26.82)	> 0.05

Abbreviation: WIR, Wash-in rate; MRE, Maximum relative enhancement; TTP, Time to peak.

using dynamic CT, the sensitivity, specificity, positive predictive value (PPV), negative predictive value (NPV), and accuracy were reported as 100%, 76.9%, 90.2%, 100%, and 92.6%, respectively for a threshold value of 20 HU (5). However, overlap in enhancement has been observed among malignant and benign masses in our study and other previous studies.

Morphologic distribution of the contrast agent related to invasion of the normal arterial system by malignant cells results in heterogeneous early enhancement. In our study, malignant masses showed heterogeneous enhancement. Tozaki et al. (25) reported prominent internal enhancement with PE for malignant masses and negligible internal enhancement with PE. Our results are in accordance with that report.

When we analyzed subgroups of malignant masses, we did not find any statistical significance. However, Schaefer et al. (4) reported that adenocarcinomas show higher MRE and faster WIR than squamous cell carcinomas. This result may be related to histological differences in vascularity between these two tumor types.

The limitations of our study were: 1, the relatively small number of benign solitary pulmonary nodules; 2, the above mentioned, time-dependent nature of the perfusion parameters and; 3, the nature of the software for the calculations. The distribution of contrast agent can be affected by the composition of the extracellular space and venous outflow, as well as the extracellular and intravascular volume fractions of the patients. Further studies on larger series are needed to achieve a better understanding of the contribution for each of these parameters.

In conclusion, in most patients with a newly detected lung mass, analysis of the morphologic features (size, contours, internal structure, and SI on conventional MR images) with clinical and laboratory data is sufficient. Our study of dynamic MR imaging of lung masses demonstrates that differentiation between benign and malignant masses is feasible. When comparing the dynamic CT examinations, the advantage of MRI is the fact that it lacks radiation exposure. We believe that the combined use of morphologic and quantitative parameters on dynamic contrast-enhanced examinations may be useful for differential diagnosis in distinct cases of lung masses.

Footnotes

Authors' Contribution: Nagihan Inan designed the overall study, collected and analyzed the data with Hasan Tahsin Sarisoy and Muhammed Donmez and co-wrote the

paper with Muhammed Donmez; Arzu ARSLAN drafted, revised, and also supervised this study.

Financial Disclosure: There is no financial disclosure.

Funding/Support: Our study did not receive any help from any organizations. It was funded by the hospital's sources.

References

1. Pauls S, Mottaghy FM, Schmidt SA, Kruger S, Moller P, Brambs HJ, et al. Evaluation of lung tumor perfusion by dynamic contrast-enhanced MRI. *Magn Reson Imaging.* 2008;**26**(10):1334–41. doi: 10.1016/j.mri.2008.04.005. [PubMed: 18538522].
2. Kono R, Fujimoto K, Terasaki H, Müller NL, Kato S, Sadohara J, et al. Dynamic MRI of Solitary Pulmonary Nodules: Comparison of Enhancement Patterns of Malignant and Benign Small Peripheral Lung Lesions. *Am J Reontgenol.* 2007;**188**(1):26–36. doi: 10.2214/ajr.05.1446.
3. Mastin ST, Drane WE, Harman EM, Fenton JJ, Quesenberry L. FDG SPECT in patients with lung masses. *Chest.* 1999;**115**(4):1012–7. [PubMed: 10208202].
4. Schaefer JF, Vollmar J, Schick F, Vonthein R, Seemann MD, Aebert H, et al. Solitary pulmonary nodules: dynamic contrast-enhanced MR imaging–perfusion differences in malignant and benign lesions. *Radiology.* 2004;**232**(2):544–53. doi: 10.1148/radiol.2322030515. [PubMed: 15215548].
5. Swensen SJ, Viggiano RW, Midthun DE, Muller NL, Sherrick A, Yamashita K, et al. Lung nodule enhancement at CT: multicenter study. *Radiology.* 2000;**214**(1):73–80. doi: 10.1148/radiology.214.1.r00ja1473. [PubMed: 10644104].
6. Yamashita K, Matsunobe S, Takahashi R, Tsuda T, Matsumoto K, Miki H, et al. Small peripheral lung carcinoma evaluated with incremental dynamic CT: radiologic-pathologic correlation. *Radiology.* 1995;**196**(2):401–8. doi: 10.1148/radiology.196.2.7617852. [PubMed: 7617852].
7. Semelka RC, Shoenut JP, Kroeker MA, Greenberg HM, Simm FC, Minuk GY, et al. Focal liver disease: comparison of dynamic contrast-enhanced CT and T2-weighted fat-suppressed, FLASH, and dynamic gadolinium-enhanced MR imaging at 1.5 T. *Radiology.* 1992;**184**(3):687–94. doi: 10.1148/radiology.184.3.1324509. [PubMed: 1324509].
8. Tanaka R, Horikoshi H, Nakazato Y, Seki E, Minato K, Iijima M, et al. Magnetic resonance imaging in peripheral lung adenocarcinoma: correlation with histopathologic features. *J Thorac Imaging.* 2009;**24**(1):4–9. doi: 10.1097/RTI.0b013e31818703b7. [PubMed: 19242296].
9. Zhang M, Kono M. Solitary pulmonary nodules: evaluation of blood flow patterns with dynamic CT. *Radiology.* 1997;**205**(2):471–8. doi: 10.1148/radiology.205.2.9356631. [PubMed: 9356631].
10. Tateishi U, Nishihara H, Watanabe S, Morikawa T, Abe K, Miyasaka K. Tumor angiogenesis and dynamic CT in lung adenocarcinoma: radiologic-pathologic correlation. *J Comput Assist Tomogr.* 2001;**25**(1):23–7. [PubMed: 11176288].
11. Metz C. ROC Methodology in Radiologic Imaging. *Invest Radiol.* 1986;**21**(9):720–33. doi: 10.1097/00004424-198609000-00009.
12. Inan N, Arslan A, Akansel G, Anik Y, Balci NC, Demirci A. Dynamic contrast enhanced MRI in the differential diagnosis of adrenal adenomas and malignant adrenal masses. *Eur J Radiol.* 2008;**65**(1):154–62. doi: 10.1016/j.ejrad.2007.03.012. [PubMed: 17466481].
13. Schima W. MRI of the pancreas: tumours and tumour-simulating processes. *Cancer Imaging.* 2006;**6**:199–203. doi: 10.1102/1470-7330.2006.0035. [PubMed: 17208676].
14. Kanematsu M, Kondo H, Goshima S, Tsuge Y, Watanabe H. Magnetic resonance imaging of hepatocellular carcinoma. *Oncology.* 2008;**75 Suppl 1**:65–71. doi: 10.1159/000173426. [PubMed: 19092274].
15. Kuhl CK, Schild HH, Morakkabati N. Dynamic bilateral contrast-enhanced MR imaging of the breast: trade-off between spatial and temporal resolution. *Radiology.* 2005;**236**(3):789–800. doi: 10.1148/radiol.2363040811. [PubMed: 16118161].
16. Fujimoto K, Abe T, Muller NL, Terasaki H, Kato S, Sadohara J, et al. Small peripheral pulmonary carcinomas evaluated with dynamic MR imaging: correlation with tumor vascularity and prognosis. *Radiology.* 2003;**227**(3):786–93. doi: 10.1148/radiol.2273020459. [PubMed: 12714678].
17. Fujimoto K. Usefulness of contrast-enhanced magnetic resonance imaging for evaluating solitary pulmonary nodules. *Cancer Imaging.* 2008;**8**:36–44. doi: 10.1102/1470-7330.2008.0009. [PubMed: 18331971].
18. Dean PB, Niemi P, Kivisaari L, Kormano M. Comparative Pharmacokinetics of Gadolinium DTPA and Gadolinium Chloride. *Invest Radiol.* 1988;**23**(1):S261. doi: 10.1097/00004424-198809000-00057.
19. Ohno Y, Hatabu H, Takenaka D, Adachi S, Kono M, Sugimura K. Solitary pulmonary nodules: potential role of dynamic MR imaging in management initial experience. *Radiology.* 2002;**224**(2):503–11. doi: 10.1148/radiol.2242010992. [PubMed: 12147849].
20. Milne ENC, Zerhouni EA. Blood supply of pulmonary metastases. *J Thorac Imaging.* 1987;**2**(4):15–23. doi: 10.1097/00005382-198710000-00005.
21. Chambers JS. Angiogenesis in lung cancer. *Ann Thorac Surg.* 1998;**66**(6):2162–3. [PubMed: 9930531].
22. Cox G. Angiogenesis and non-small cell lung cancer. *Lung Cancer.* 2000;**27**(2):81–100. doi: 10.1016/s0169-5002(99)00096-3.
23. Duarte IG, Bufkin BL, Pennington MF, Gal AA, Cohen C, Kosinski AS, et al. Angiogenesis As A Predictor Of Survival After Surgical Resection For Stage I Non-Small-Cell Lung Cancer. *J Thorac Imaging.* 1998;**115**(3):652–9. doi: 10.1016/s0022-5223(98)70331-9.
24. Fontanini G, Vignati S, Boldrini L, Chine S, Silvestri V, Lucchi M, et al. Vascular endothelial growth factor is associated with neovascularization and influences progression of non-small cell lung carcinoma. *Clin Cancer Res.* 1997;**3**(6):861–5. [PubMed: 9815760].
25. Tozaki M, Ichiba N, Fukuda K. Dynamic magnetic resonance imaging of solitary pulmonary nodules: utility of kinetic patterns in differential diagnosis. *J Comput Assist Tomogr.* 2005;**29**(1):13–9. [PubMed: 15665676].